A Hybrid Submicroscopic-Microscopic Traffic Flow Simulation Framework

Mullakkal-Babu, Freddy; Wang, Meng; van Arem, Bart; Shyrokau, Barys; Happee, Riender

DOI
10.1109/TITS.2020.2990376

Publication date
2021

Document Version
Final published version

Published in
IEEE Transactions on Intelligent Transportation Systems

A Hybrid Submicroscopic-Microscopic Traffic Flow Simulation Framework

Freddy Antony Mullakkal-Babu, Meng Wang, *Member, IEEE*, Bart van Arem, *Senior Member, IEEE*, Barys Shyrokau, and Riender Happee

***Abstract*— Current lane-based microscopic traffic simulators combine car-following and lane changing logic to describe the (often discrete) lateral vehicle motion on multi-lane road segments. However, the simulated lateral trajectories are physically unplausible and inside-lane behavior such as lane-keeping and curve negotiation cannot be modelled. In this work, we integrate lateral vehicle dynamics and yaw motion into a traffic simulation framework, aiming to describe lateral motion and vehicle interactions with more precision. The resulting framework consists of two coupled layers, an upper tactical level that plans maneuvers such as lane-changing; and a lower operational layer with a control module (steering and acceleration control) that operates in a closed loop with the bicycle model of vehicle dynamics. The feedback mechanism between the layers allows for dynamic trajectory re-planning. Unlike the microscopic traffic models, the proposed framework accounts for lateral vehicle dynamics and yaw motion; provides additional variables such as vehicle heading and front wheel steering angle; and is hence termed as submicroscopic. Case study results demonstrate the power of the framework to include lateral maneuvers such as curve negotiation, corrective steering, lane change abortion and fragmented lane changing. The framework was operationalized to model multi-lane traffic flow consisting of human-driven vehicles. At the macroscopic level, the traffic flow simulation can reproduce phenomena such as capacity drop. Thus the framework preserves the properties of the component models and at the same time describe the continuous 2-D planar movement of vehicles.**

***Index Terms*— Traffic model, submicroscopic, microscopic, hybrid, multilane.**

I. Introduction

MICROSCOPIC traffic models aim to describe the movement of individual vehicles in traffic. Microscopic models for longitudinal vehicle dynamics mostly use follow-the-leader logic. Such models describe the longitudinal vehicle motion as an outcome of dynamic interaction with the preceding vehicles [1]. They have been applied to analyze the properties of single-lane traffic flow such as motorway capacity and platoon stability. In a multi-lane traffic environment, vehicles perform a planar motion (longitudinal, lateral and yaw motion). Therefore a longitudinal model must be combined with a counterpart lateral model to describe maneuvers such as lane-changing and lane-keeping. Microscopic models of lateral movement mostly focus on the lane change decision (LCD). LCD models describe the decision-making process as an outcome of interactions with ambient traffic and driver's intrinsic preferences [2], [3]. A typical microscopic traffic simulator for multi-lane traffic integrates a longitudinal car-following model and a lateral lane-change decision model to generate 2-D vehicle trajectories. It employs a simplified vehicle model to efficiently simulate a large number of vehicles necessary to test traffic management strategies and to evaluate the traffic flow impacts of longitudinal automation systems such as Adaptive Cruise Control. The simplified vehicle models employed by microscopic simulators, however, do not necessarily yield plausible trajectories of lateral maneuvers, during which the dynamic constraints of vehicle motion come to play. Considering that the lateral maneuvers such as lane changes are frequently observed on multi-lane motorways, realistically modeling them is relevant to ensure accurate results, especially regarding traffic safety [4], [5].

The simplified representation of lateral vehicle dynamics reflects four methodological deficiencies. Firstly, an explicit vehicle model is not included in the modeling framework; instead, the driver and vehicle are treated as a single unit [6]. Hence, such simulators do not ensure that the driver-vehicle unit respects the nonholonomic constraints of the vehicle motion [4]. Moreover, they do not differentiate the motion behavior of vehicles based on physical properties such as mass and inertial properties. The second deficiency is the absence of a steering angle which is an essential control variable for lateral maneuvers such as lane-changing. Alternatively, most of the simulators interpolate the lateral vehicle position during the lane change event, which is typically treated as an instantaneous event [7] upon which the vehicle jumps from one lane to the other or as a fixed-duration process within which the vehicle achieves a lateral displacement [4], [8]. Considering that the number of positive lane change decisions depends explicitly on the simulation time-step and the lane

Manuscript received February 15, 2019; revised September 29, 2019 and February 10, 2020; accepted March 23, 2020. Date of publication May 6, 2020; date of current version June 2, 2021. This work was supported by the Nederlandse Organisatie voor Wetenschappelijk Onderzoek (NWO) Domain Toegepaste en Technische Wetenschappen (TTW), The Netherlands, through the Project from Individual Automated Vehicles to Cooperative Traffic Management–Predicting the benefits of automated driving through on-road human behaviour assessment and traffic flow models (IAVTRM) under Grant TTW 13712. The Associate Editor for this article was M. Brackstone. *(Corresponding author: Meng Wang.)*

Freddy Antony Mullakkal-Babu, Meng Wang, and Bart van Arem are with the Faculty of Civil Engineering and Geosciences, Delft University of Technology, 2628 Delft, The Netherlands (e-mail: f.a.mullakkalbabu@tudelft.nl; m.wang@tudelft.nl; b.vanarem@tudelft.nl).

Barys Shyrokau is with the Faculty of Mechanical, Maritime and Materials Engineering, Delft University of Technology, 2628 Delft, The Netherlands (e-mail: b.shyrokau@tudelft.nl).

Riender Happee is with the Faculty of Civil Engineering and Geosciences, Delft University of Technology, 2628 Delft, The Netherlands, and also with the Faculty of Mechanical, Maritime and Materials Engineering, Delft University of Technology, 2628 Delft, The Netherland (e-mail: r.happee@tudelft.nl).

Digital Object Identifier 10.1109/TITS.2020.2990376

change duration, this approach can influence the number of simulated lane changes. Moreover, this treatment regards lane-changing as an open-loop process. Once a lane change decision is made, neither the lane change decision nor the movement is re-evaluated. On the contrary, behavioral studies on human-steering control report that lane changing is a closed-loop process in which drivers use visual feedback to regulate the steering operation [9], [10]. The major problem with this approach, however, is that the dependency between lateral and longitudinal vehicle state variables is not accounted for.

The aforementioned deficiencies restrict or detriment the applicability of such simulators for safety assessment of traffic involving lateral vehicle maneuvers. Safety metrics such as the surrogate safety measures are directly quantified from the simulated trajectories [4], [5]. If the trajectories are unrealistic, the safety assessments are prone to be inaccurate. Besides, lateral maneuvers such as aborted lane changing and interrupted lane changing cannot be described by existing microscopic simulators, as they involve feedback between the steering operation and the lane change decision. Inaccurate modeling of lane changes can detriment the validity of estimation of lane change-induced impacts. Moreover, current microscopic simulators, which lack a steering angle description, do not allow direct modeling of steering controllers and are not suitable to assess their impacts.

Recently, modeling frameworks that integrate an explicit vehicle dynamic model with microscopic models have been proposed. Due to their detailed description of vehicle dynamics, they are known as submicroscopic or nanoscopic models [1], [11]. Compared to microscopic simulators, submicroscopic simulators improve the realism of simulated trajectories. Kumar *et al*. [12] proposed a multi-level modelling framework based on bond-graphs incorporating detailed longitudinal dynamics. Dedes *et al*. [13] proposed a framework that integrates the vehicle dynamics and GNSS-INU errors. Moreover, PELOPS [14] is a commercial software package that allows detailed modeling of longitudinal dynamics. Such submicroscopic models, however, do not explicitly model vehicle dynamics in the lateral maneuver. So *et al*. [4] proposed an approach to generate more realistic lateral maneuver trajectories. In this approach, targeted for traffic safety assessment, lateral trajectories from a microscopic model are post-processed by a high-fidelity commercial vehicle model [4], [15]. However this approach is not adequate to analyze the effects of lateral maneuvers on traffic flow characteristics. Kaths and Krause [16] proposed a co-simulation framework wherein a single test vehicle is modeled by a high fidelity commercial vehicle model, and the surrounding vehicles are simulated by the microscopic model. None of the reviewed works attempts to model the multi-lane traffic flow wherein all the simulated trajectories respect vehicle dynamic constraints.

The objective of this work is to propose and operationalize a framework to model multi-lane traffic flow with 2-D trajectory descriptions of vehicles by integrating driving-task-specific models (decision-making and operation) with an explicit vehicle model. Such a framework is envisioned to improve the accuracy of traffic safety assessment. The framework adopts a modular architecture to allow implementing and testing of independent models specific to various driving sub-tasks. This paper focuses on modeling human-driven vehicles, while future publications will address mixed traffic with human driven and automated vehicles. The resulting framework consists of two coupled layers: an upper tactical level that generates dynamic maneuver plans; and a lower operational layer with explicit control module (front road-wheel steering and acceleration control) that operates in a closed loop with the bicycle model of vehicle dynamics. The simulator employs a hybrid scheme to reduce the computational load. To enhance computational efficiency, it activates the maneuver planning and steering control only during lateral maneuvers such as lane changing and curve negotiation, and performs as a microscopic simulator otherwise.

In this work, we propose a means to integrate lateral vehicle dynamics into the traffic simulation framework. In comparison to the typical simulation approaches, the presented framework has three advantages: 1) by incorporating the bicycle model for lateral dynamics in traffic simulation, the proposed framework captures the effects of vehicle model parameters on lateral dynamics and yaw motion and thereby improves the realism of the simulation 2) the framework can model a wider set of vehicle maneuvers: the steering control module allows modelling curve negotiation, corrective steering; and closed-loop interconnection between tactical and operational layer allows modelling aborted and fragmented lane changes 3) the submicroscopic variables such as front road-wheel steering and vehicle heading angle allow examinaing the feasibility of the behavioral sub-models.

The mathematical formulations of the framework are presented in Section II and the framework is operationalized using existing behavioral models in Section III. The integrated performance of the framework and the results of traffic flow simulations are presented in Section IV. The limitations and possibilities of the framework are discussed in Section V, and finally, the conclusions are presented in Section VI.

II. Model Framework

In order to meet the research objective the framework design should meet three requirements: 1) it should be generic to include human-driven and automated vehicles; 2) it should be modular to allow testing of multiple models that independently focus on specific driving tasks, such as lane change decisions or car following; 3) it should be able to describe front road-wheel steering and acceleration variables subject to vehicle dynamics.

A. Framework

The framework consists of two coupled layers: an upper *tactical plan* layer and a lower *operational control* layer as shown in Figure 1. The constituent layers were conceptually proposed by Michon [17]. The proposed framework complements the conceptual framework by laying a solid mathematical foundation that operationalizes on-road driving tasks accounting for feedback in and between different layers. Besides, this framework is consistent with the decision and control system

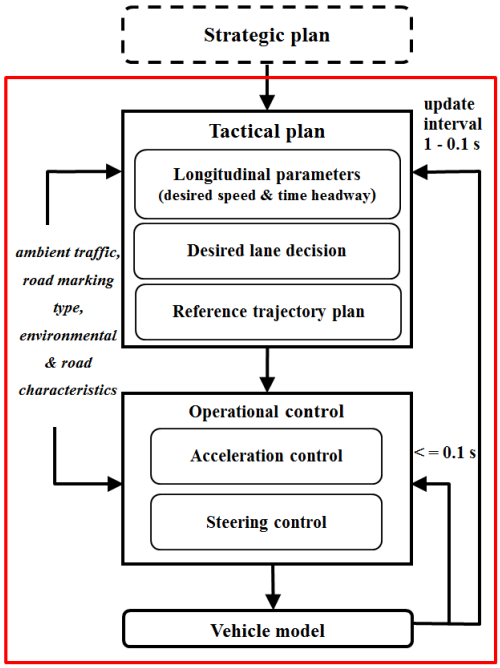

Fig. 1. Framework for hybrid submicroscopic-/microscopic simulation, the red box indicates the scope of this work.

architecture applied for highly automated vehicles [18] and therefore satisfies requirement 1.

To meet requirement 2, the framework adopts a modular architecture. The influence of strategic plans such as route and destination choices is beyond the current research scope and therefore the strategic plan layer is omitted. The upper tactical layer generates dynamic decisions and plans pertaining to the vehicle maneuvers. For the longitudinal driving task, the tactical layer sets the parameters such as desired velocity and desired time headway to desired values. The dynamic decision pertaining to lateral maneuvers is the desired lane which is generated by the *desired lane* module. The vehicle performs a lane change maneuver if a lane other than the current lane is desired. In this case, the *reference trajectory* module generates the reference plan to facilitate the lane-changing maneuver. This can be a static plan over a time horizon or a dynamic plan updated at each time step. For lane-changing, the horizon is in the order of few seconds (typically < 10 s). Additionally, the tactical commands governing the lane change should ensure the safety of a prospective lane change. Most of the behavioral lane change decision models serve this purpose as they include a safety check prior to accepting a gap in the desired lane. In automated vehicles, this safety check is typically performed by the reference trajectory module.

The operational layer generates control commands (i.e. acceleration and front road-wheel steering angle), respecting the tactical decisions, to operate the vehicle along the reference trajectory. This layer consists of a *steering control* module and an *acceleration control* module which generates the front road-wheel steering and acceleration commands respectively, thereafter the vehicle state is updated subject to the dynamic behavior described by the *vehicle model* module. The operational control commands are usually updated at the fraction of one second, a frequency much higher than the tactical layer decisions. The tactical and operational functions will be specifically formulated later in this section.

In this framework, the information is circulated between the two control layers and the vehicle system (represented by the system dynamic model) in order to model the revisions in maneuver plans, eg, trajectory replanning or aborting a lane-change. The tactical plan is updated at a time-step Δt^u and the operational actions are updated at time-step Δt^l such that $\Delta t^u \geq \Delta t^l$. The kinematic states and properties of ambient traffic entities such as vehicles, road markings, and road characteristics enter the framework as environmental inputs at the tactical and operational layers.

The presented framework differs from most microscopic frameworks on two aspects: 1) the existence of an explicit vehicle model and steering control, 2) the existence of a feed-back mechanism between the tactical and operational layers. The component modules in the framework allow modeling the lateral and longitudinal dynamics and yaw motion of individual vehicles in multi-lane traffic flow. Even though the two-layered structure is a well-known conceptual framework, in this contribution, we establish the component modules and construct the relationship between the component modules. This allows the modeling of driver-vehicle behaviors that cannot be captured in the microscopic framework such as dynamic trajectory planning and maneuvers such as curve negotiation, corrective steeting, fragmented lane change and lane change abortion. We demonstrate the operations of the framework as a prototype simulator for human-driven vehicles.

B. Vehicle Model

In this section, we specify the vehicle model used in the framework. The vehicle motion is modeled as a loosely coupled combination of two linearized models describing the longitudinal; and lateral and yaw motion.

1) Model for Longitudinal Vehicle Dynamics: Let (x) denote the longitudinal position of the vehicle based coordinate system as shown in Figure 2, then its longitudinal dynamics can be expressed as

$$m\ddot{x} = F_T - F_A - F_G - F_D \tag{1}$$

where m denotes the physical mass of the vehicle, F_T denotes the traction force, F_R denotes the aerodynamic drag, F_G denotes grade resistance and F_D denotes the mechanical drag. The longitudinal dynamics expressed in (1) can be modeled in a linear form by employing exact linearization. We refer to [19] for its detailed mathematical derivation. The following set of differential equations describe the linearized longitudinal model

$$\frac{d}{dt}\begin{Bmatrix} x \\ \dot{x} \\ \ddot{x} \end{Bmatrix} = \begin{Bmatrix} v_x \\ a_x \\ \dfrac{u_x - a_x}{\tau} \end{Bmatrix} \tag{2}$$

where v_x denotes the longitudinal velocity and a_x denotes the actual longitudinal acceleration. The longitudinal motion is controlled by the desired acceleration command u_x.

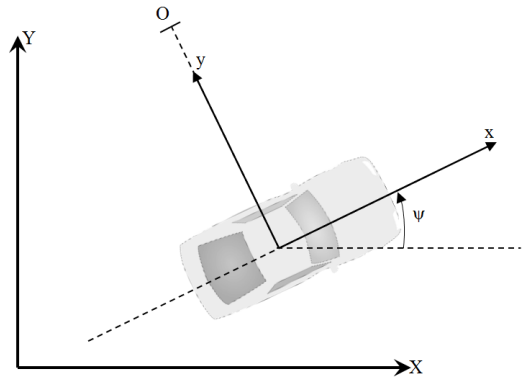

Fig. 2. The two coordinate systems and the motion variables.

The desired acceleration is executed with a lag: τ representing the finite time needed by the engine actuators to generate the desired acceleration. The physical limitations of vehicle motion are implemented as a set of constraints: we model strictly forward motion and feasible velocity limit by setting $0 < v_x < v^{max}$; we bound the acceleration representing the powertrain limitations and braking systems as $-a_{brake} \leq a_x \leq a_{acc}$.

2) Model for Lateral Vehicle Dynamics: The classical dynamic 'bicycle' model [20] is chosen to model the lateral vehicle dynamics. This linear time-invariant model has been widely used in the design of steering controllers [21], [22] and has been shown to demonstrate a good modeling accuracy [23]. First, the equation for the translational motion of the vehicle can be derived from Newton's second law of motion as follows

$$m\left(\ddot{y} + \dot{\psi} v_x\right) = F_{yf} + F_{yr} \tag{3}$$

where m denotes the mass of the vehicle. The inertial acceleration of the vehicle's center of gravity in the y-direction (see Fig. 2) is the algebraic sum of the acceleration $\ddot{y}$ along the y-axis and the centripetal acceleration $\dot{\psi} v_x$; ψ is the heading angle of the vehicle in the global X-Y coordinate system. The two front wheels and the two rear wheels are represented by a single front and rear wheel, and F_{yf}, F_{yr} are the lateral tire forces of the figurative single front and rear wheels respectively. The equation for yaw dynamics is obtained by the moment balance about the z-axis as

$$I_z \ddot{\psi} = l_f F_{yf} - l_r F_{yr} \tag{4}$$

where I_z denotes the moment of inertia about the z-axis; l_f, l_r denotes the respective distances of the front and rear axles from the center of gravity. The lateral tire forces in (3) are approximated by linear functions of slip angles [20] as

$$F_{yi} = 2C_i \alpha_i, \quad i \in \{f, r\} \tag{5}$$

where f and r denote the front and rear axle respectively, C_i is the cornering stiffness of lumped tires for the axle i, and α_i is the slip angle of lumped tire i. At small angles, α_i can be approximated as

$$\alpha_f = \theta_f - \frac{\dot{y} + l_f}{v_x}, \quad \alpha_r = \frac{l_r - \dot{y}}{v_x} \tag{6}$$

where θ_f is the front road-wheel steering angle. The small angle approximation is reasonable for typical highway operating conditions. Substituting (5) and (6) into (4) and (3), the state space model for lateral motion can be written as

$$\dot{\mathbf{s_y}} = \mathbf{A}\mathbf{s_y} + \mathbf{B}\theta_\mathbf{f} \tag{7}$$

where

$$\mathbf{s_y} = \begin{bmatrix} y \\ \dot{y} \\ \psi \\ \dot{\psi} \end{bmatrix}, \quad \mathbf{B} = \begin{bmatrix} 0 \\ \dfrac{2C_{\alpha f}}{m} \\ 0 \\ \dfrac{2l_f C_{\alpha f}}{I_z} \end{bmatrix}$$

$$\mathbf{A} = \begin{bmatrix} 0 & 1 & 0 & 0 \\ 0 & -\dfrac{2C_{\alpha f} + 2C_{\alpha r}}{m v_x} & 0 & -v_x - \dfrac{2l_f C_{\alpha f} - 2l_r C_{\alpha r}}{m v_x} \\ 0 & 0 & 0 & 1 \\ 0 & -\dfrac{2l_f C_{\alpha f} - 2l_r C_{\alpha r}}{I_z v_x} & 0 & -\dfrac{2{l_f}^2 C_{\alpha f} + 2{l_r}^2 C_{\alpha r}}{I_z v_x} \end{bmatrix}$$

According to this model, the lateral vehicle position y and the heading angle ψ is controlled by the front road-wheel steering input θ_f.

C. Formulating Tactical Functions

In this section, we specify the tactical functions and formulate models to represent them. Figure 3 depicts the tactical planning process in the framework. The function of the tactical layer is to generate the reference input vector $\mathbf{R} = \left(v^d, T^d, \xi(t), k(t)\right)^T$. The first two elements are longitudinal reference inputs: v^d denotes the desired velocity during unconstrained driving. The second input, T^d denotes the desired time gap with the preceding vehicle on the desired lane σ^*. Here, v^d and T^d are dynamic variables that are revised to describe the temporary behavioral changes. For instance, v^d is revised to reflect the change in speed limit or T^d is reduced to reflect acceptance of shorter time headways during lane-changing. We select these two variables as the tactical reference signals governing the longitudinal motion, as they are commonly present in a wide range of phenomenological car following models [24] and longitudinal control systems such as Adaptive Cruise Control [25]. The third and fourth elements are the lateral reference inputs. $\xi(t)$ denotes the direction of lane change i.e. $\{-1, -0.5, 0, 0.5, 1\}$:= change to the center of the left lane, move to left boundary, no change, move to the right boundary, change to the center of the right lane. Here, $\xi(t) = \pm 0.5$ represents the driver's decision to temporally pause the lateral maneuver by driving roughly along the lane boundary. Such fragmented maneuvers are executed by human drivers [26] and are applied as a lane change strategy in highly automated driving systems [18]. For human driven vehicles, the $\xi(t)$ can be modelled by existing lane change decision models, and their detailed review can be found in [27]. $k(t)$ denotes the curvature of the reference trajectory plan as follows

$$k(t) = \begin{cases} k_\sigma, & \text{if: } \xi(t) = 0 \\ k(t) \forall t_0 \leq \mathrm{t} \leq t_0 + \overline{D}, & \text{if: } \xi(t) \neq 0 \end{cases} \tag{8}$$

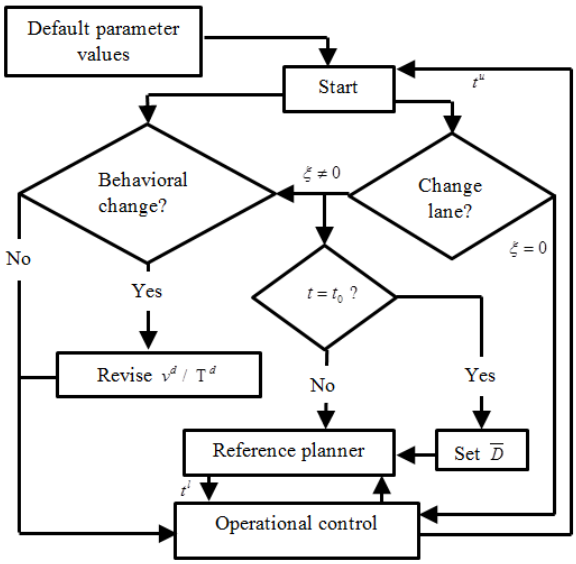

Fig. 3. Flowchart of tactical planning.

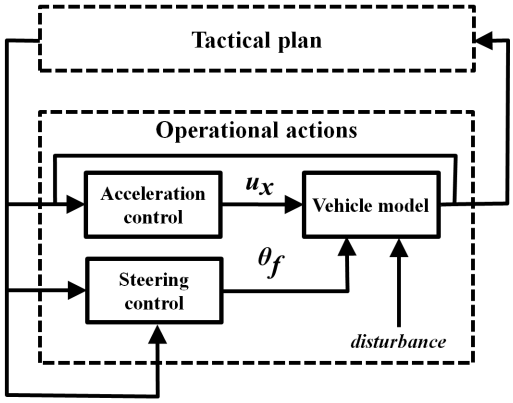

Fig. 4. Control structure implemented in the framework.

where k_σ is the curvature of the center line of the current lane, σ; t_0 is the current time, $\overline{D}$ is the lane change duration. The models to describe the aforementioned tactical inputs will be specified in Section III.

D. Formulating Operational Functions

The function of the operational layer is to generate front road-wheel steering θ_f and acceleration commands u_x. The block diagram of the adopted control structure is shown in Fig. 3. The control problem is divided into two subproblems and we deploy two interconnected controllers to solve each problem. The longitudinal controller generates the acceleration command u_x to track the longitudinal reference input and lateral controller accounts for the velocity change induced by the longitudinal control and generates front road-wheel steering command to regulate the vehicle to track the reference path specified by the reference curvature input.

III. Operationalization of the Framework With Behavioral Models

In this section, we operationalize the framework to describe trajectories of human-driven vehicles on a multi-lane road stretch. Towards this, we select a set of established behavioral models to be applied as component modules of the framework.

A. Models of Tactical Functions

This section details the chosen behavioral models to describe tactical reference inputs.

1) Longitudinal Parameters: The two tactical inputs governing the longitudinal dynamics are: v^d denoting the desired speed and T^d denoting the desired time headway. The value of v^d is fixed for each driver and is bounded by the maximum feasible speed v^{max}. Similary, T^d is a fixed value, and is temporarily adjusted during a mandatory lane change. During a mandatory lane change, the lane-changing vehicle (c) and the following-vehicle on the target lane (f) accepts a shorter headway to facilitate the lane change and subsequently relaxes to the normal headway within a finite time horizon [28]. In this work, the variation of T^d during the relaxation horizon is modelled as a linear rise [2].

2) Lane Change Decision: The lane change decision is described by the model: Minimising Overall Braking Induced by Lane changes (MOBIL). The model description and validation can be found in [3]. This model specifies compact rules that govern the lane-change decisions of human drivers. This model derives the utility and risk of a lane change from a car-following model and is compatible with a wide range of car-following models. This model accounts for the car-following acceleration of three vehicles: the lane changing vehicle c, follower vehicle in the current lane o and potential follower in the target lane f. In this model, the utility of a lane change is defined as

$$U = \widetilde{A}_c - A_c + p\left[\widetilde{A}_f - A_f + \widetilde{A}_o - A_o\right] \tag{9}$$

where A_c is the acceleration of c in the current lane and $\widetilde{A}_c$ is its acceleration after the prospective lane change. Similarly, the current and prospective accelerations of the original follower o and potential follower f are included in the model. The parameter p denotes the politeness parameter representing the degree of cooperation while considering a lane change: $p = 0$ implies egoistic behavior without considering the implication to neighboring vehicles and $p > 1$ implies an altruistic one. The lane change decision is then made based on the following rule

$$\xi(t) = \begin{cases} +1 : U_{right} > \Delta A_{th} - A_{bias} \quad \& \quad U_{right} \geq U_{left} \\ -1 : U_{left} > \Delta A_{th} + A_{bias} \quad \& \quad U_{left} > U_{right} \\ 0 : \text{otherwise} \end{cases} \tag{10}$$

where A_{bias} implements the keep-right directive on lane usage, A_{th} the threshold of overall acceleration gain.

3) Reference Plan for a Lane Change Trajectory: In order to generate $k(t)$ when $\xi(t) \neq 0$, a reference trajectory planner should be deployed. Since the tactical layer operates in a closed loop with the operational layer, the reference trajectory plan should allow dynamic updates. We use a time-based polynomial function to formulate the reference trajectory. This function has been used to formulate reference plans in

automated lane change control systems [22]. The reference trajectory is planned as an independent time series of the vehicle global lateral and longitudinal positions as follows

$$\begin{aligned} Y(t) &= a_5t^5 + a_4t^4 + a_3t^3 + a_2t^2 + a_1t + a_0 \\ X(t) &= b_2t^2 + b_1t + b_0 \end{aligned} \tag{11}$$

The reference lateral trajectory is chosen to be a quantic polynomial as it allows a continuous curvature and is differentiable to the third degree. The reference longitudinal trajectory is chosen to be a quadratic polynomial so as to represent the constant longitudinal acceleration generated by the longitudinal controller. The above functions include nine unknown coefficients which can be determined by solving for the boundary conditions of the lane change process in (12), thereby smoothly connecting the preceding and following driving period.

$$\begin{aligned} X(t) &= X_0, \quad \dot{X}(t) = V_{X,0}, \ \ddot{X}(t) = A_{X,0} \\ Y(t) &= Y_0, \quad \dot{Y}(t) = V_{Y,0}, \ \ddot{Y}(t) = A_{Y,0} \\ Y(D) &= Y_D, \quad \dot{Y}(D) = 0, \ \ddot{Y}(D) = 0 \end{aligned} \tag{12}$$

where $X_0, V_{X,0}, A_{X,0}$ are the current global longitudinal position, velocity and acceleration; $Y_0, V_{Y,0}, A_{Y,0}$ are the current global lateral position, velocity and acceleration; Y_D is the final lateral position and D is the remaining time duration to complete the lane change. Applying the boundary conditions in (14) to (13), the nine unknowns can be formulated as a function of D and Y_D. The curvature of the reference trajectory can be derived as a function of time as follows

$$k(t) = \frac{\ddot{Y}(t)\dot{X}(t) - \ddot{X}(t)\dot{Y}(t)}{\dot{X}(t)^3\left(1 + \left(\frac{\dot{Y}(t)}{\dot{X}(t)}\right)^2\right)^{\frac{3}{2}}} \tag{13}$$

The tactical variation in desired lane change direction $\xi_i(t)$ governed by (10) will be reflected in Y_D as follows: $Y_D(t) = Y_\sigma + W\xi_i(t)$, where Y_σ is the lateral position of the centerline of the current lane, σ; W is the lane width; and as we model lane changes as fixed duration maneuvers, we set $D = \overline{D} - t$.

4) Lane Change Duration: The duration of each lane change event is treated as a variable that is derived from the traffic conditions at the start of the lane change. We choose the model proposed by Toledo and Zohar [29] to describe the lane change duration of a vehicle. This model guarantees a non-negative lane change duration but does not constrain its maximum value. Therefore, the lane change duration is restricted to maximum value $D^{\max}$

$$\bar{D}_n = \min(e^{\beta E_n}, D^{\max}) \tag{14}$$

where E_n denotes the vector of explanatory variables including traffic density and relative kinematic states of the subject vehicle with respect to the follower and leader in the target lane. β is a vector consisting of the weights assigned to each explanatory variable.

B. Models of Operational Functions

This section details the chosen behavioral models to describe the acceleration and front road-wheel steering commands.

1) Acceleration Control: To describe the acceleration control of human drivers, we employ the behavioral model: Intelligent Driver Model [30] with descriptive parameters. The IDM acceleration of a vehicle is a continuous function of space gap and velocity difference of n with the preceding vehicle $n-1$.

$$u_x = a\left[1 - \left(\frac{\dot{X}_n}{v^d}\right)^4 - \left(\frac{s^*(\dot{X}_n, \Delta\dot{X}_n)}{s_n}\right)^2\right] \tag{15}$$

where a denotes the maximum acceleration, v^d is the desired velocity obtained as the reference command, $s_n = X_{n-1} - X_n - L$ denotes the space gap, L denotes the length of the $n-1$, $\Delta\dot{X}$ denotes the velocity difference of n with respect to the preceding vehicle $n-1$. s^* denotes the desired minimum gap as follows

$$s^* = s_0 + \dot{x}T^d + \frac{\dot{x}}{2\sqrt{ab}} \tag{16}$$

where T^d is the desired time headway that is obtained as the reference sigal from tactical layer, s_0 denotes the minimum space gap, and b is the comfortable braking.

2) Steering Control: We choose a steering controller with state feedback to describe the steering control [20], [31]. The controller regulates the front road-wheel steering angle by tracking the error: **e** described as follows

$$\mathbf{e} = \begin{bmatrix} e_1 \\ e_2 \end{bmatrix} \in e_1 = y - y_{ref}; \quad e_2 = \psi - \psi_{ref} \tag{17}$$

where y_{ref} is the vehicle based lateral coordinate of the reference trajectory (during lane changing) or the centerline of the current lane (during lane keeping), ψ_{ref} is the reference heading angle which is the angle between the horizontal axis and the tangent of the reference path at y. The front road-wheel steering signal is obtained by a state feedback vector **K** in combination with a feedforward term θ_{ff} providing feedforward control of the desired curvature as follows:

$$\theta_f = -\mathbf{Ke} + \theta_{ff} \tag{18}$$

where θ_{ff} is derived from the steady state steering angle for zero lateral position error as given in [20]. By inserting the steering control law to the vehicle dynamics model in (7), we can derive the closed loop state feedback system as:

$$\frac{d}{dt}\{\mathbf{e}\} = \left[\mathbf{A^c} - \mathbf{B_1^c K}\right]\{\mathbf{e}\} + \left[\mathbf{B_2^c}\right]\dot{\psi}_{ref} + \left[\mathbf{B_1^c}\right]\theta_{ff} \tag{19}$$

where $\dot{\psi}_{ref}$ is the reference yaw rate is derived from the reference curvature command from (13) using the relationship $\dot{\psi}_{ref} = v_x k$. $\mathbf{A^c}$, $\mathbf{B_1^c}$, $\mathbf{B_2^c}$ are the closed loop system matrices parameterized by the vehicle static vehicle parameters as

follows

$$\mathbf{A^c} = \begin{bmatrix} 0 & 1 & 0 & 0 \\ 0 & -\dfrac{2C_{\alpha f}+2C_{\alpha r}}{m v_x} & \dfrac{2C_{\alpha f}+2C_{\alpha r}}{m} & \\ 0 & 0 & 0 & 1 \\ 0 & -\dfrac{2l_f C_{\alpha f}-2l_r C_{\alpha r}}{I_z v_x} & \dfrac{2l_f C_{\alpha f}-2l_r C_{\alpha r}}{I_z} & \\ & 0 & & \\ & -\dfrac{2l_f C_{\alpha f}-2l_r C_{\alpha r}}{m v_x} & & \\ & 1 & & \\ & -\dfrac{2l_f{}^2 C_{\alpha f}+2l_r{}^2 C_{\alpha r}}{I_z v_x} & & \end{bmatrix}$$

$$\mathbf{B_1^c} = \begin{bmatrix} 0 \\ \dfrac{2C_{\alpha f}}{m} \\ 0 \\ \dfrac{2l_f C_{\alpha f}}{I_z} \end{bmatrix}, \quad \mathbf{B_2^c} = \begin{bmatrix} 0 \\ -v_x - \dfrac{2l_f C_{\alpha f}-2l_r C_{\alpha r}}{m v_x} \\ 0 \\ -\dfrac{2l_f{}^2 C_{\alpha f}+2l_r{}^2 C_{\alpha r}}{I_z v_x} \end{bmatrix} \tag{20}$$

Applying the optimal state feedback vector $\mathbf{K}$ in (18) minimises the performance index J defined as

$$J = \sum_{K=0}^{\infty} \mathbf{e^T(K)Qe(K)} + \theta_\mathbf{f}^\mathbf{T}\mathbf{(K)R}\theta_\mathbf{f} \tag{21}$$

where J is a quadratic measure of future behavior with origin as the target. Here, $\mathbf{Q}$ is the weight of deviation of the state from the target and $\mathbf{R}$ is the weight of the control activity. The optimal feedback $\mathbf{K}$ in (21) is derived from $\mathbf{S}$ which is solution of the associated algebraic Ricatti equation by setting

$$\mathbf{K} = \mathbf{R^{-1}}(\mathbf{B_1^{cT}S}) \tag{22}$$

The solution of $\mathbf{K}$ in (22) is obtained by a Linear Quadratic Regulator algorithm. The global coordinates of the vehicle can be estimated as $X = \int_0^t v_x \cos(\psi_{ref})dt - e_1 \sin(e_2 + \psi_{ref})$ and $Y = \int_0^t v_x \sin(\psi_{ref})dt + e_1 \cos(e_2 + \psi_{ref})$ [20].

IV. Simulation Experiment and Results

The framework and the selected formulations of the component models of the prototype simulator were presented in the previous section in a continuous time form. In this section, we numerically implement the hybrid framework using discrete time simulations. The tactical layer is updated at $\Delta t^u = 0.1$ s and the operational layer is updated at $\Delta t^l = 0.01$ s. To reduce the computional load, the acceleration commands are estimated at an interval of 0.1 s. We evaluate the performance of the integrated framework and prototype traffic flow simulation by two separate sets of simulation experiments performed in MATLAB. In the first set, the modeling framework is evaluated based on the simulation results of scenario case studies consisting of few vehicles. In the second experiment, the prototype is evaluated by simulating the human-driven traffic flow comprised of 2000 vehicles on a two-lane freeway section with an onramp bottleneck.

A. Evaluating the Modelling Framework

To verify the performance of the modelling framework, we designed three test cases. First, we evaluate the sensitivity of uncontrolled lateral vehicle dynamics towards the vehicle model parameters. In the second test, we evaluate the steering operation in two scenarios: curve negotiation and corrective steering. Finally, in the third test, we evaluate lane change trajectories including dynamic reference replanning such as aborted lane change and fragmented lane change. The default vehicle model parameters are set as follows: $m = 1573$ kg; $I_z = 2873$ kg.m^2; $C_{\alpha f} = C_{\alpha r} = 80000$ N/rad; $l_f = 1.1$ m; $l_r = 1.58$ m. These values correspond to a passenger sedan [20]. The results are compared to a similar experiment reported in [32].

1) Evaluating the Sensitivity of the Vehicle Model: Fig. 5 depicts the vehicle yaw dynamics under an initial steering input $\theta_f = 0.1$ rad. This illustrates the sensitivity of the vehicle yaw dynamics to the vehicle parameters of mass, the moment of inertia, the center of mass and velocity. An increase in the mass of the vehicle reduces the steady-state yaw rate and reduces its damping in transient response (see Fig. 5(a)). Thereby, this model will represent heavier vehicles as less steerable, which is intuitive. An increase in the moment of inertia increases the settling time indicating a slower time responses (see Fig. 5(b)). This behavior is also intuitive, for example, sports cars are designed with a low moment of inertia for faster time response. As the center of mass moves toward the vehicle front, the time response is seen to be quicker (see Fig. 5(c)). Finally, the forward velocity is a key parameter that influences the vehicle handling (see Fig. 5(d)). The steady-state vehicle yaw rate increases with an increase in velocity until a critical point (around 40 m/s for the selected vehicle parameters), and the steady state response decreases with increase in the velocity beyond the point. The modeled behavior is consistent with empirical observations and with previous studies [32]. The selected parameters are capable of modeling a representative vehicle operating at freeway conditions.

2) Evaluating the Performance of the Operational Layer: Inaccurate steering control is a major factor contributing to single-vehicle accidents on motorway horizontal curves, and corrective oversteering can lead to vehicle crashes [9], [33]. Even though this aspect has been being reported in accident studies, conventional microscopic traffic simulation models are incapable to capture them. In this context, we evaluate the ability of the framework to model control related errors. In this experiment, we simulate two distinct steering operational tasks: curve negotiation and corrective steering. The tactical reference vector for the curve negotiation is as follows $v^d = 30$ m/s;

$$k(t) = \begin{cases} 0 \in 0 < t < 0.5 \\ 1/750 \in t \geq 0.5. \end{cases}$$

The change in reference curvature $k(t)$ reflects the change in road geometry: from a straight stretch to a horizontal curve of radius 750 m when $t \geq 0.5$ s. The initial vehicle state is as follows: $X(0) = Y(0) = 0$; $V_X(0) = 30$; $V_Y(0) = 0$; $\psi(0) = 0$; $\dot{\psi}(0) = 0$.

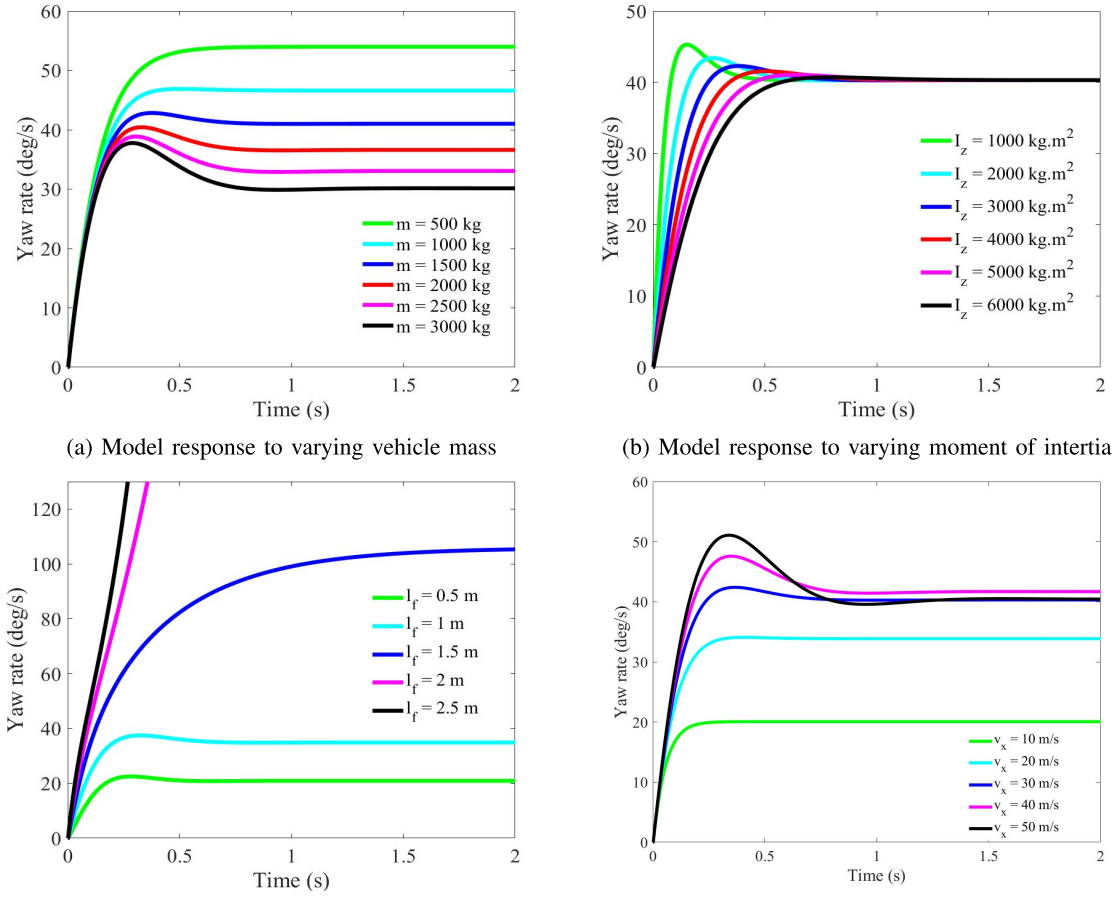

(a) Model response to varying vehicle mass

(b) Model response to varying moment of intertia

(c) Model response to shifting the center of gravity away from the front wheel

(d) Model response to varying velocity

Fig. 5. Step response of the vehicle model with varying model parameters.

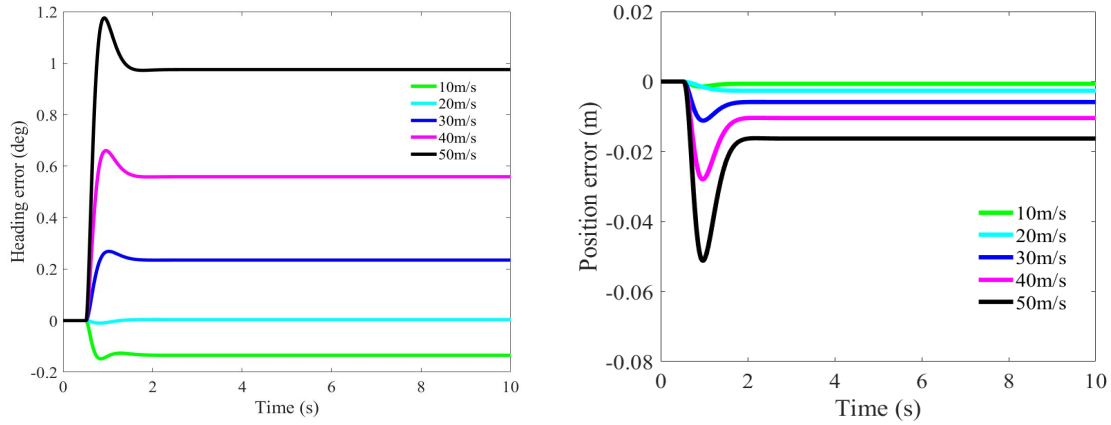

(a) Heading error with varying velocity

(b) Position error with varying velocity

Fig. 6. Simulated steering operation during curve negotiation.

The simulation results in Fig. 6 show that the operational model is able to capture the control related error while negotiating a horizontal curve. It can be seen, that negotiating the curve at higher velocities induces a larger position error (see Fig. 6(a)) and heading angle error (see Fig. 6(b)) defined in (17). Therefore, the modelled curve negotiations at high velocity result in a larger tracking error, which is consistent with the empirical observation that over-speeding is a common characteristic underlying single vehicle accidents at motorway curves [33]–[35].

The corrective steering is the maneuver undertaken when the vehicle has (perhaps inadvertently) disoriented itself with the road center line and has to steer back in order to realign with the road centerline. Here, we consider a straight road stretch

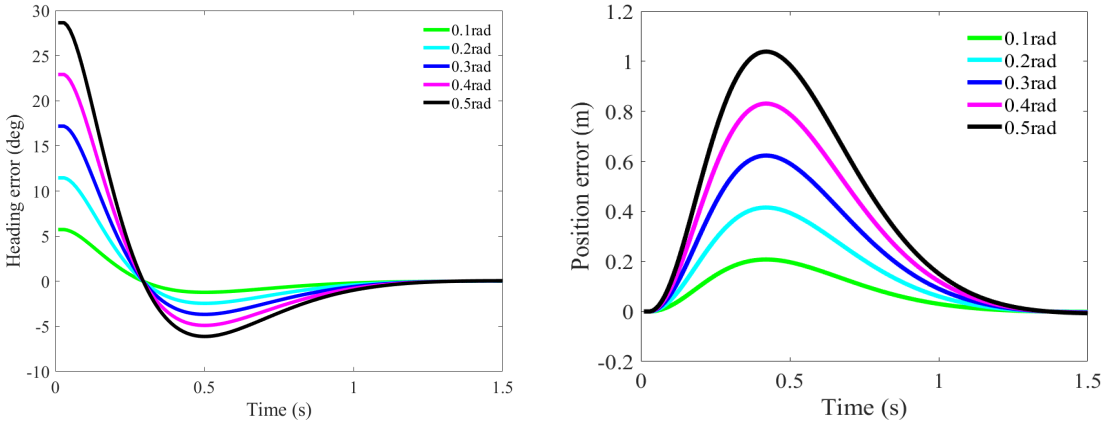

(a) Heading error with varying initial heading angle (b) Position error with varying initial heading angle

Fig. 7. Simulated steering operation during corrective steering.

and vehicle's tactical reference input is $v^d = 30$ m/s. The initial state of the vehicle except for the heading angle (varied) is as follows: $X(0) = Y(0) = 0$; $V_X(0) = 30$; $V_Y(0) = 0$; $\dot{\psi}(0) = 0$. The initial heading angle is varied from 0.1 to 0.5 rad.

The simulation results in Fig. 7 show that steering amplitude and the settling time (see Fig. 7(a)) increase with initial heading error. This is consistent with human corrective steering performance examined in driving simulators [9].

3) Evaluating the Lane Change Simulation: The ability of the framework to model lane changes, is evaluated by three different scenario simulations resulting in different types of lane change execution. All three scenarios involve a subject vehicle (right lane), leader and preceding vehicles (left lane).

The first scenario describes a normal lane change to a slower lane. Initially, the subject vehicle moves at 30 m/s and the two neighbouring vehicles are at 20 m/s. The leader in the target lane applies a constant deceleration of -1 m/s^2 till 5 s. Meanwhile, the subject vehicle initiates a lane change at 4 s, simultaneously decelerating to follow the leader (see Fig. 8(a) and Fig. 8(b)). It can be seen that the vehicle sucessfully completes the lane change in the next 5 s (see Fig. 8(c)), re-align with the target lane ($\psi = 0$ from 9 s in Fig. 8(e)), to continue driving on it (see Fig. 8(d) and Fig. 8(f)).

The second and third scenarios describe an aborted lane change and a fragmented lane change respectively. These maneuvers present interesting examples of maneuver replanning by human drivers [26]. To meet the objective of this test, we define exemplary rule-based decision-making logic that allows to abort or interrupt a pre-initiated lane change as follows

$$\xi_i(t) = \begin{cases} \xi_i(t_0) & if: A_{X,i}(t), A_{X,i+1}(t) > A^* \\ 0.5\xi_i(t_0) & if: A_{X,i+1}(t) < A^* \\ 0, & if: A_{X,i}(t) < A^* \end{cases} \quad (23)$$

where $\xi_i(t_0)$ is the desired lane change direction of the vehicle i at the start of the lane change, i denotes the lane changing vehicle, $i+1$ and $i-1$ denotes the rear and leading vehicle in the target lane respectively. $A_{X,i}(t)$ is the acceleration signal provided by the longitudinal controller of i to follow $i-1$, and

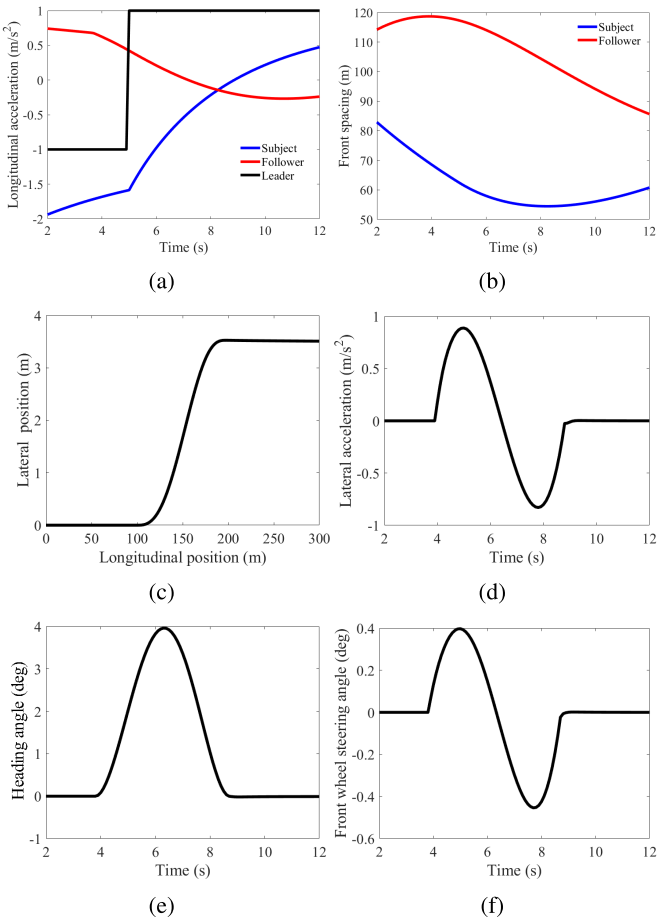

Fig. 8. Simulated lateral and longitudinal dynamics during a normal lane change to the slower lane.

$A_{X,i+1}(t)$ is the acceleration signal generated by the longitudinal controller of $i+1$ to follow i, A^* denotes the deceleration threshold which is set as -2 m/s^2. The logic of the rule (24) is as follows: if the longitudinal acceleration input of both i and $i+1$ remain in the comfortable range ($> A^*$), then the lane change is sustained uninterrupted; if longitudinal acceleration input of $i+1$ drops lower than the comfortable range ($\leq A^*$)

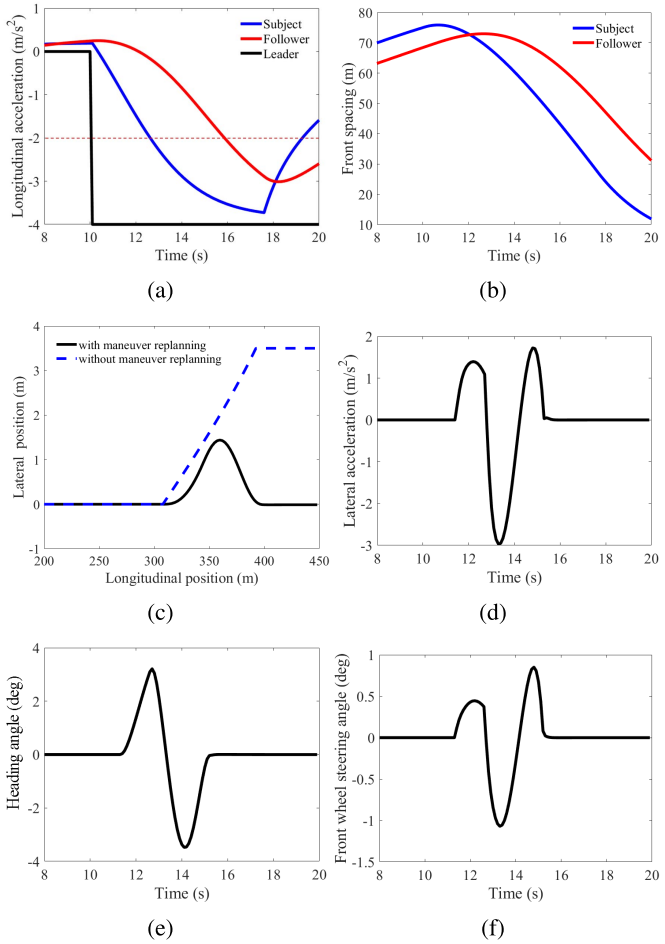

Fig. 9. Simulated lateral and longitudinal dynamics during an aborted lane change.

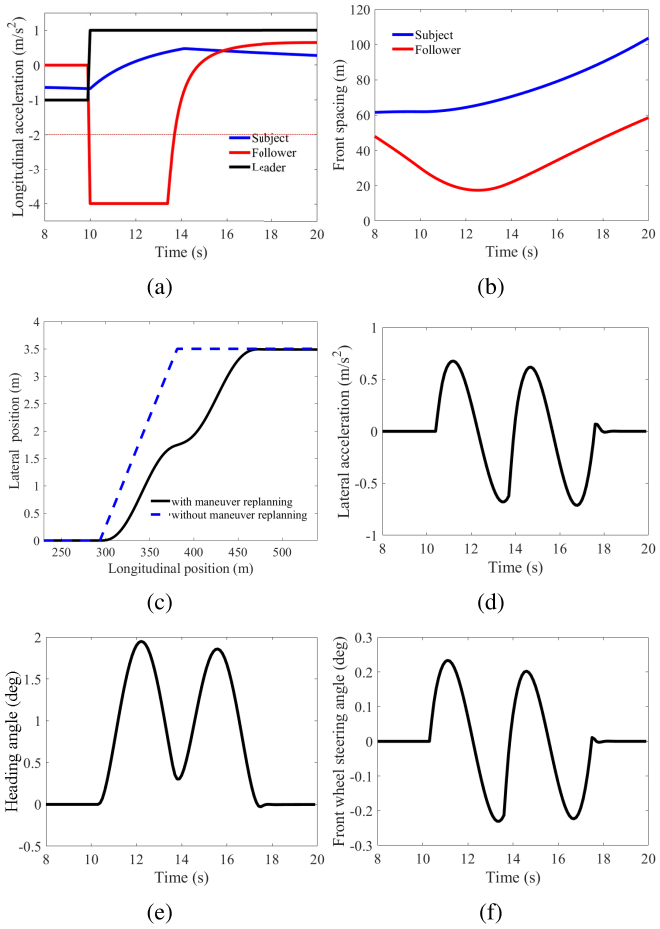

Fig. 10. Simulated lateral and longitudinal dynamics during a fragmented lane change.

at some point, then i temporarily pauses the lateral maneuver and waits for $i+1$ to cooperate by decelerating, and proceeds with the lateral maneuver when the demanded $A_{X,i+1}(t)$ is comfortable; if the longitudinal acceleration input of i drops lower than the comfortable range at some point, the maneuver is aborted and i returns to its original lane. Besides, when the lane changing is temporarily paused, i.e. $\xi_i(t) = \pm 0.5$, the $\overline{D}$ has to be extended to $\overline{D}^*$ in order to accommodate the intermediate delay, where $\overline{D}^* = \overline{D} + t^p$. Here t^p denotes the intermediate pause time.

In the second scenario, we consider an aborted lane change. Initially, all three vehicles move at 30 m/s. The leading vehicle in the target lane applies an abrupt deceleration of -4 m/s^2 starting after 10 s (see Fig. 9(a) and Fig. 9(b)). The subject vehicle initiates the lane change at 11.5 s; however, as its longitudinal acceleration drops below A^* at 12.7 s (see red dotted line in Fig. 9(a)), its tactical layer commands to abort the lane change based on (23) and consequently swerves back to the original lane. Fig. 9 shows the detailed description of the maneuvre provided by the proposed framework. It can be seen that the vehicle moves back to the original lane (see Fig. 9(c)), and re-align with the original lane ($\psi = 0$ from 15 s in Fig. 9(e)), to continue driving on it (see Fig. 9(d) and Fig. 9(f)). In a typical microscopic simulator, the lane-changing vehicle moves with constant lateral velocity of 1 m/s without dynamic maneuver replanning. This would result in the blue-dashed trajectory in Fig. 9(c). It can be seen that without maneuver replanning, the simulation outcome of this situation would be different, and the lane-changer would end up in the target lane. Moreover, the lateral acceleration along this trajectory is discontinuous at the start and endpoint of the lane-changing due to a step-change in lateral velocity.

In the third scenario, we consider fragmented lane changing. Initially, all three vehicles move at 35 m/s. Initially, the leader applies constant deceleration of -1 m/s^2 till 10 s and thereafter applies an acceleration of 1 m/s^2. Additionally, we set the following vehicle acceleration as 0 m/s^2 till 10 s, implying that it does not react to the decceleration of the subject vehicle till that point. Thereafter its longitudinal controller is engaged and it begins to follow the subject vehicle (see Fig. 10(a) and Fig. 10(b)). Meanwhile, the subject vehicle initiates the lane change at 10.5 s. As the desired acceleration of the follower is below A^*, its tactical layer commands a temporary pause in lane change based on (23). After a pause of 3.3 s, the desired acceleration of the follower is above A^* at 13.7 s (see red dotted line in Fig. 10(a)), and the tactical layer commands to resume the maneuver to the right

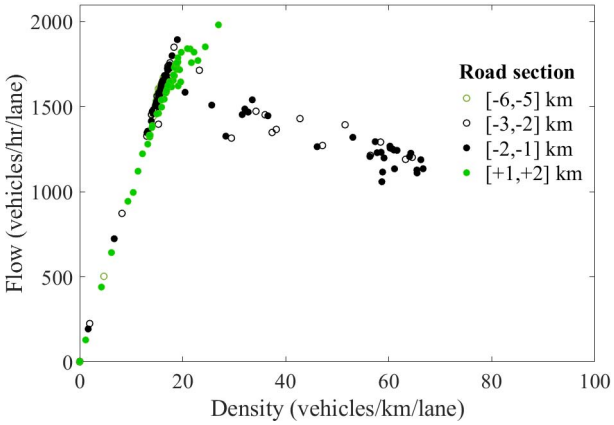

Fig. 11. Macroscopic traffic flow with varying density.

lane based on (23). Fig. 10 shows the detailed maneuver description. It can be seen that the vehicle reaches the target lane (see Fig. 10(c)), aligns with the target lane ($\psi = 0$ from 18 s in Fig. 10(e)) and continues driving on it (See Fig. 10(d) and Fig. 10(f)). Fig. 10(c) shows the simulation of this situation without maneuver replanning. As the time consumed by the intermediate pause cannot be modelled, the lane changer ends up in the target lane earlier, similar to a continuous lane change.

B. Evaluating the Prototype Traffic Flow Simulation

In this section, we evaluate the prototype traffic flow simulation specified in section III. To this end, a two-lane road section of 9.2 km long with open boundary conditions was simulated. The inflow at the upstream boundary was kept constant at 1,600 vehicles/h/lane. The lane width is 3.5 m, a standard for Dutch motorways. Furthermore, the road stretch consists of an on-ramp (merging length 200 m) at the location x = 7.2 km with a constant inflow of 800 vehicles/h. In order to simplify the analysis, we omit heavy vehicles in the simulation which can introduce distinct effects on traffic flow characteristics. As specified in section III, the modules in the prototype traffic flow simulation are described by existing behavioral models, which have been empirically validated. The prototype does not include models for aborted and fragmented lane changes. The simulation period is 1800 s. The parameter values used in the simulation are listed in Table I. The vehicle parameter values are the same as detailed in section IV. A. To reduce the computational load, the prototype traffic flow simulation, employs a hybrid scheme, wherein the trajectory planning and steering control modules (updated at a high frequency of 0.01 s) are activated only when a lane change is initiated, otherwise, it functions as a normal microscopic simulation.

1) Macroscopic Variables: Fig. 11 shows the simulated macroscopic flow characteristics. The flow and density were calculated using Edie's definitions [36] for a stretch of 1 km and time interval of 30 s. The diagram captures well known macroscopic traffic flow properties. Fig. 11 shows both the free flow regime and congested traffic state. It can be seen that the traffic on the road stretches downstream (green dots

TABLE I
PARAMETER VALUES IN THE PROTOTYPE TRAFFIC FLOW SIMULATION

Parameter (description)	Value
a (IDM maximum acceleration)	1 m/s^2
b (IDM comfortable braking)	1.5 m/s^2
v^{max} (IDM maximum speed)	160 km/hr
v^d (IDM desired velocity)	108 km/hr
T^d (IDM desired time headway)	1 s
s_0 (IDM minimum space gap	2 m
$D^{\max}$ (maximum lane change duration)	8 s
τ (actuator lag)	0 s *
A_{bias} (MOBIL bias parameter)	0.2
p (MOBIL politeness parameter)	0.15
ΔA_{th} (MOBIL acceleration threshold)	0.2

* τ = 0 to preserve the behavioral properties of IDM

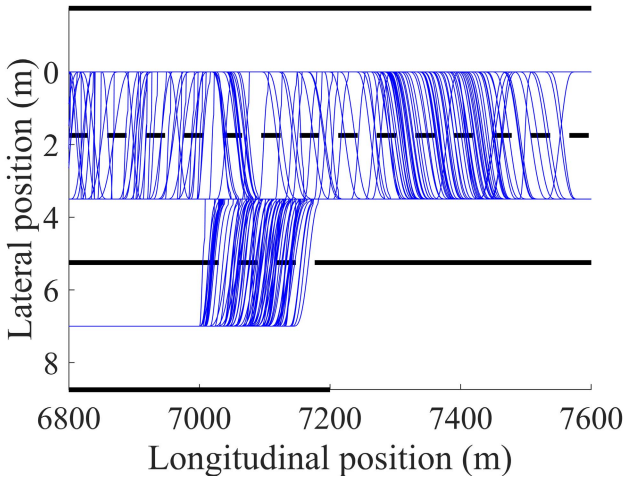

Fig. 12. Simulation results; blue lines indicate vehicle trajectories and black lines indicate lane boundaries.

in Fig. 11) and further upstream of the bottleneck (green circles in Fig. 11) are in a free flow state. The stationary congested traffic occurs around the bottleneck and stop and go waves propagate upstream with a velocity of −14 km/hr. This is observed in road stretches in the upstream vicinity of the bottleneck (black dots and circles in Fig. 11). The transition from free flow state to congested state occurs approximately at 20 veh/km, which can be considered as the critical density. The values of stop and go wave velocity and critical density are consistent with empirical observations [24]. It can be seen in Fig. 11 that near the maximum flow the points are arranged in the shape of an inverse λ, implying the existence of both free and congested states around the critical density. The corresponding reduction in the maximum flow is around 10% and is consistent with the empirical observations of 5 - 20% [24], [37].

2) Microscopic and Submicroscopic Variables: The vehicle trajectories near the onramp section are shown in Fig. 12. The simulation resulted in 1178 lane changes. It can be seen that the number of lane changes increases in the vicinity of the onramp entrance (7000 - 7200 m). The number of lane changes is relatively higher on the road segment immediately

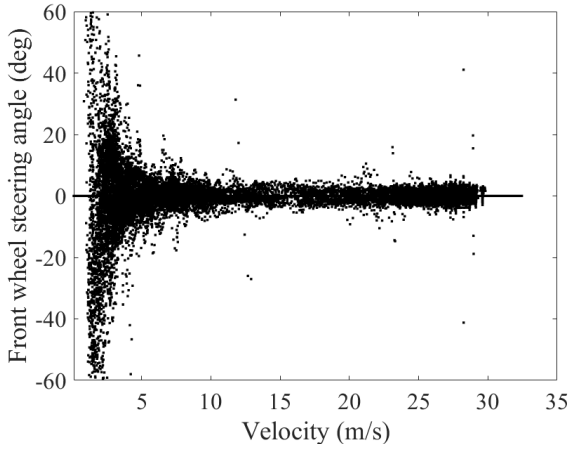

Fig. 13. Distribution of front wheel steering angle with varying longitudinal velocity.

downstream (7200 - 7500 m) of the bottleneck, caused by vehicles moving to the right lane after the bottleneck. This could be the result of right lane bias implemented in the lane change decision model. The number of lane changes is relatively lower on the road segment further away from the merge (7500 - 8500 m) as the traffic here is predominantly in the free flow state (see Fig. 11).

Fig. 13 shows the distribution of steering angle with varying longitudinal velocity. It can be seen that at high-velocity regimes the front wheel steering angle remains within $\pm 10^{\circ}$ and at lower velocity, distribution of steering angles scatters to higher value. These outliers shall be addressed in future model versions.

V. Discussion

We presented the framework to model human-driven traffic flow by operationalizing the component modules with existing behavioral models. The longitudinal vehicle dynamics was described using the IDM car-following model, which has been empirically validated [30]. In order to preserve the properties of the behavioral car-following model, the actuator lag τ was set to zero. This parameter may be assigned a finite value to represent the vehicle motion by automated acceleration controllers such as Adaptive Cruise Control [25], [38].

Few lane change trajectories in the simulation were found to be infeasible, i.e $\theta_f > \pm 70^{\circ}$. These trajectories were observed when the longitudinal velocity dropped to 0 - 1 m/s. Since the safety concerns at this velocity range are marginal, such lane change trajectories were overridden with linear interpolations of lateral positions during the lane change duration. A possible reason is that the lane change duration used in the reference plan is estimated from a behavioral model that does not explicitly account for the trajectory feasibility. Moreover, the steering commands were not explicitly constrained. This highlights the necessity for further empirical research on path planning by the human drivers at such low velocities.

The present framework could be improved by adding behavioral parameters characterizing the human drivers such as (variable) response time and perception error [39]. Van Lint and Calvert [40] proposed a theory to model the perception and response processes at tactical and operational layers. They implemented this theory for car-following dynamics. Zheng *et al*. [41] modeled the changes in car-following behavior induced by lane changing. The presented framework describes lateral interactions during lane-changing. However, to describe interactions over a longer horizon such as during weaving and merging maneuvers in congested traffic [2], [7]. Such interactions can be incorporated in the framework by extending the planning horizon and reformulating the tactical planner with corresponding models.

Even though detailed trajectory descriptions are beneficial for traffic applications, the high computational demand is a major obstacle to its real-time application. In this study, we reduced the demand by employing a hybrid scheme, wherein the high-frequency update was only performed during lane changing. Besides we selected linear models for lateral and longitudinal dynamics. Thereby, the simulator could operate at real-time speed (run-time $=$ 1 s, meaning that the simulator takes 1 second to simulate 1 second of traffic flow) with up to 100 active vehicles on the road. The run-time increased to 5 s with 440 active vehicles and further up to 10 s with 900 active vehicles. The run-time can be lowered by operating the simulator in a parallel or distributed computing system. Another possible step is to restrict the submicroscopic simulation to complex segments such as crossroads or merging sections.

In this study, the parameters of the component models were selected from their original papers. However, the parameters should be calibrated based on the simulator application. The level of detail to be considered in the calibration should depend on the objective of the analysis. In a safety assessment study, the surrogate safety metrics are extracted directly from the simulated trajectories and therefore the calibration might be restricted to microscopic variables [5]. High resolution trajectory datasets such as the one by Wagner *et al.* [42] provide opportunities for such calibration attempts. On the contrary, if one is interested in the performance evaluation of a steering control system, then the parameters related to submicroscopic variables should be calibrated.

The presented simulation framework has several potential applications: 1) Assessing the safety impacts of driving applications such as Automated Lane-Changing Systems and Automated Lane Keeping Systems. This can be done by formulating the tactical planner and operational control with respective modules of the systems. 2) Investigating the effects of lateral vehicle control on traffic characteristics, such as the capacity drop at motorway horizontal curves. This can be done by operationalising the steering control module with a human steering model which can be developed from driving simulator experiments [9]. 3) Examining the relationship between road design parameters and traffic safety at traffic facilities such as motorway discontinuities and intersections which are typically characterised by frequent lane changes including fragmented and aborted lane changes [26]. 4) Comparing the performance of alternative crash-avoidance applications in different vehicle types in uncontrolled traffic situations involving dynamic vehicle interactions.

Even though the modelling framework is not restricted to highway traffic, for other traffic scenarios the selection and parameterisation of constituent models might have to be adapted. For instance, urban traffic features distinct driver behaviour for which the model parameters should be calibrated, and the tactical layer must be reformulated to generate low speed maneuver plans entailing large steering angles and to account for the anticipatory behaviour while approaching a traffic signal.

VI. Conclusion

We presented a method to integrate vehicle lateral dynamics and yaw motion into the traffic modelling framework, and thereby to enhance the simulation detail with submicroscopic variables such as vehicle heading and front wheel steering angle. We mathematically formulated the functions and dependencies of the various models within the framework. The results of simulation case studies in Section IV provide a proof-of-concept demonstration of the benefits of the framework. At the macroscopic level, the multi-lane traffic flow simulation could reproduce well-known traffic flow properties such as critical density and phenomena such as a capacity drop. Simulation examples demonstrate the limitation of typical microscopic simulation approaches to describe lateral maneuvers involving dynamic trajectory replanning. In contrast, the proposed submicroscopic framework can simulate such lateral maneuvers: curve negotiation, corrective steering, fragmented and aborted lane-changing. Thus the framework preserves the properties of the component models and at the same time describe the 2D planar movement of vehicles.

As detailed in the discussion section, there exist multiple prospects to improve the framework, such as incorporating the behavioral aspects of human-driven vehicles and devising an appropriate computational paradigm to allow real-time simulation. Our future work will focus on the aforementioned tasks.

Acknowledgment

The authors would like to thank Dr. Wouter Schakel for his contribution in setting up the simulation environment.

References

[1] S. P. Hoogendoorn and P. H. L. Bovy, "State-of-the-art of vehicular traffic flow modelling," *Proc. Inst. Mech. Eng., I, J. Syst. Control Eng.*, vol. 215, no. 4, pp. 283–303, Jun. 2001.

[2] W. J. Schakel, V. L. Knoop, and B. van Arem, "Integrated lane change model with relaxation and synchronization," *Transp. Res. Rec., J. Transp. Res. Board*, vol. 2316, no. 1, pp. 47–57, Jan. 2012.

[3] A. Kesting, M. Treiber, and D. Helbing, "General lane-changing model MOBIL for car-following models," *Transp. Res. Rec.,J. Transp. Res. Board*, vol. 1999, no. 1, pp. 86–94, Jan. 2007.

[4] J. So, B. Park, S. M. Wolfe, and G. Dedes, "Development and validation of a vehicle dynamics integrated traffic simulation environment assessing surrogate safety," *J. Comput. Civil Eng.*, vol. 29, no. 5, Sep. 2015, Art. no. 04014080.

[5] F. A. Mullakkal-Babu, M. Wang, H. Farah, B. van Arem, and R. Happee, "Comparative assessment of safety indicators for vehicle trajectories on highway," *Transp. Res. Rec*, vol. 2659, pp. 127–136, 2017.

[6] J. Barceló, "Models, traffic models, simulation, and traffic simulation," in *Fundamentals of Traffic Simulation* (International Series in Operations Research & Management Science), J. Barceló, Ed. New York, NY, USA: Springer, 2010, ch. 2, pp. 63–95.

[7] P. Hidas, "Modelling vehicle interactions in microscopic simulation of merging and weaving," *Transp. Res. C, Emerg. Technol.*, vol. 13, no. 1, pp. 37–62, Feb. 2005.

[8] M. Fellendorf and P. Vortisch, "Microscopic traffic flow simulator VISSIM," in *Fundamentals of Traffic Simulation*. New York, NY, USA: Springer, 2010, pp. 63–93.

[9] D. D. Salvucci and R. Gray, "A two-point visual control model of steering," *Perception*, vol. 33, no. 10, pp. 1233–1248, Oct. 2004.

[10] L. Li, C. Lv, D. Cao, and J. Zhang, "Retrieving common discretionary lane changing characteristics from trajectories," *IEEE Trans. Veh. Technol.*, vol. 67, no. 3, pp. 2014–2024, Mar. 2018.

[11] D. Ni, "2DSIM: A prototype of nanoscopic traffic simulation," in *Proc. IEEE IV Intell. Vehicles Symposium*, Jun. 2003, pp. 47–52.

[12] P. Kumar, R. Merzouki, B. Conrard, V. Coelen, and B. O. Bouamama, "Multilevel modeling of the traffic dynamic," *IEEE Trans. Intell. Transp. Syst.*, vol. 15, no. 3, pp. 1066–1082, Jun. 2014.

[13] G. Dedes *et al.*, "Integrated GNSS/INU, vehicle dynamics, and microscopic traffic flow simulator for automotive safety," in *Proc. 14th Int. IEEE Conf. Intell. Transp. Syst. (ITSC)*, Oct. 2011, pp. 41–53.

[14] J. Ludmann, D. Neunzig, and M. Weilkes, "Traffic simulation with consideration of driver models, theory and examples," *Vehicle Syst. Dyn.*, vol. 27, nos. 5–6, pp. 491–516, Jun. 1997.

[15] H. Park, C. S. Bhamidipati, and B. L. Smith, "Development and evaluation of enhanced IntelliDrive-enabled lane changing advisory algorithm to address freeway merge conflict," *Transp. Res. Rec., J. Transp. Res. Board*, vol. 2243, no. 1, pp. 146–157, Jan. 2011.

[16] J. Kaths and S. Krause, "Integrated simulation of microscopic traffic flow and vehicle dynamics," in *Proc. IPG Apply Innovate Conf.*, Karlsruhe, Germany, Feb. 2016.

[17] J. A. Michon, "A critical view of driver behavior models: What do we know, what should we do," *Human Behavior and Traffic Safety*. Boston, MA, USA: Springer, 1985, pp. 485–520.

[18] M. Ardelt, C. Coester, and N. Kaempchen, "Highly automated driving on freeways in real traffic using a probabilistic framework," *IEEE Trans. Intell. Transp. Syst.*, vol. 13, no. 4, pp. 1576–1585, Dec. 2012.

[19] M. Wang, "Infrastructure assisted adaptive driving to stabilise heterogeneous vehicle strings," *Transp. Res. C, Emerg. Technol.*, vol. 91, pp. 276–295, Jun. 2018.

[20] R. Rajamani, "Lateral Vehicle Dynamics," in *Vehicle Dynamics and Control*, 2nd ed., F. F. Ling, Ed. Boston, MA, USA: Springer, 2012, ch. 2, pp. 12–46.

[21] C. Hatipoglu, U. Ozguner, and K. A. Redmill, "Automated lane change controller design," *IEEE Trans. Intell. Transp. Syst.*, vol. 4, no. 1, pp. 13–22, Mar. 2003.

[22] Y. Luo, Y. Xiang, K. Cao, and K. Li, "A dynamic automated lane change maneuver based on vehicle-to-vehicle communication," *Transp. Res. C, Emerg. Technol.*, vol. 62, pp. 87–102, Jan. 2016.

[23] D. E. Smith and J. M. Starkey, "Effects of model complexity on the performance of automated vehicle steering controllers: Model development, validation and comparison," *Vehicle Syst. Dyn.*, vol. 24, no. 2, pp. 163–181, Mar. 1995.

[24] M. Treiber and A. Kesting, *Traffic Flow Dynamics*. Berlin, Germany: Springer, 2013.

[25] F. A. Mullakkal-Babu, M. Wang, B. van Arem, and R. Happee, "Design and analysis of full range adaptive cruise control with integrated collision a voidance strategy," in *Proc. IEEE 19th Int. Conf. Intell. Transp. Syst. (ITSC)*, Nov. 2016, pp. 308–315.

[26] D. Yang, L. Zhu, F. Yang, and Y. Pu, "Modeling and analysis of lateral driver behavior in lane-changing execution," *Transp. Res. Rec., J. Transp. Res. Board*, vol. 2490, no. 1, pp. 127–137, Jan. 2015.

[27] Z. Zheng, "Recent developments and research needs in modeling lane changing," *Transp. Res. B, Methodol.*, vol. 60, pp. 16–32, Feb. 2014.

[28] J. A. Laval and L. Leclercq, "Microscopic modeling of the relaxation phenomenon using a macroscopic lane-changing model," *Transp. Res. B, Methodol.*, vol. 42, no. 6, pp. 511–522, Jul. 2008.

[29] T. Toledo and D. Zohar, "Modeling duration of lane changes," *Transp. Res. Rec., J. Transp. Res. Board*, vol. 1999, no. 1, pp. 71–78, Jan. 2007.

[30] M. Treiber, A. Hennecke, and D. Helbing, "Congested traffic states in empirical observations and microscopic simulations," *Phys. Rev. E, Stat. Phys. Plasmas Fluids Relat. Interdiscip. Top.*, vol. 62, no. 2, pp. 1805–1824, Aug. 2000.

[31] Z. Lu, B. Shyrokau, B. Boulkroune, S. van Aalst, and R. Happee, "Performance benchmark of state-of-the-art lateral path-following controllers," in *Proc. IEEE 15th Int. Workshop Adv. Motion Control (AMC)*, Mar. 2018, pp. 541–546.

[32] M. Mondek and M. Hromcik, "Linear analysis of lateral vehicle dynamics," in *Proc. 21st Int. Conf. Process Control (PC)*, Jun. 2017, pp. 240–246.
[33] M. Staubach, "Factors correlated with traffic accidents as a basis for evaluating advanced driver assistance systems," *Accident Anal. Prevention*, vol. 41, no. 5, pp. 1025–1033, Sep. 2009.
[34] W. H. Schneider, P. T. Savolainen, and K. Zimmerman, "Driver injury severity resulting from single-vehicle crashes along horizontal curves on rural two-lane highways," *Transp. Res. Rec., J. Transp. Res. Board*, vol. 2102, no. 1, pp. 85–92, Jan. 2009.
[35] L. Li, G. Lai, and F. Y. Wang, "Safe steering speed estimation and optimal trajectory planning for intelligent vehicles," in *Proc. IEEE Netw., Sens. Control*, Mar. 2005, pp. 722–727.
[36] L. C. Edie, "Car-following and steady-state theory for noncongested traffic," *Oper. Res.*, vol. 9, no. 1, pp. 66–76, Feb. 1961.
[37] M. J. Cassidy and R. L. Bertini, "Some traffic features at freeway bottlenecks," *Transp. Res. B, Methodol.*, vol. 33, no. 1, pp. 25–42, Feb. 1999.
[38] H. A. Rakha, K. Ahn, W. Faris, and K. S. Moran, "Simple vehicle powertrain model for modeling intelligent vehicle applications," *IEEE Trans. Intell. Transp. Syst.*, vol. 13, no. 2, pp. 770–780, Jun. 2012.
[39] M. Treiber, A. Kesting, and D. Helbing, "Delays, inaccuracies and anticipation in microscopic traffic models," *Phys. A, Stat. Mech. Appl.*, vol. 360, no. 1, pp. 71–88, Jan. 2006.
[40] J. W. C. van Lint and S. C. Calvert, "A generic multi-level framework for microscopic traffic simulation—Theory and an example case in modelling driver distraction," *Transp. Res. B, Methodol.*, vol. 117, pp. 63–86, Nov. 2018.
[41] Z. Zheng, S. Ahn, D. Chen, and J. Laval, "The effects of lane-changing on the immediate follower: Anticipation, relaxation, and change in driver characteristics," *Transp. Res. C, Emerg. Technol.*, vol. 26, pp. 367–379, Jan. 2013.
[42] P. Wagner, R. Nippold, S. Gabloner, and M. Margreiter, "Analyzing human driving data an approach motivated by data science methods," *Chaos, Solitons Fractals*, vol. 90, pp. 37–45, Sep. 2016.

Freddy Antony Mullakkal-Babu received the bachelor's degree in civil engineering from the National Institute of Technology, Calicut, in 2011, and the master's degree in transportation systems engineering from the Indian Institute of Technology Bombay, Mumbai, in 2014. He is currently pursuing the Ph.D. degree with the Department of Transport and Planning, Delft University of Technology. His main research interests include driver behavior modeling, traffic safety, and design and assessment of driving automation systems.

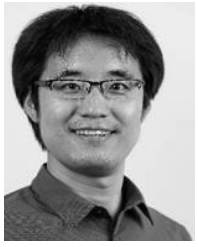

Meng Wang (Member, IEEE) received the M.Sc. degree in transportation engineering from the Research Institute of Highway, China, in 2006, and the Ph.D. degree in transport and planning from the Delft University of Technology, The Netherlands, in 2014. From 2014 to 2015, he was a Post-Doctoral Researcher with the Department of Biomechanical Engineering, Delft University of Technology, where he has been an Assistant Professor with the Department of Transport and Planning since 2015. His main research interests include driving behavior modeling, traffic flow, and control approaches for cooperative driving systems.

Bart van Arem (Senior Member, IEEE) received the master's degree in 1986 and the Ph.D. degree in applied mathematics, with a specialty in queuing theory, from the University of Twente, The Netherlands, in 1990. He was a Researcher and a Program Manager in intelligent transport systems with TNO from 1992 to 2009, where he was involved in various national and international projects. Since 2009, he has been a Full Professor with the Department of Transport and Planning, Delft University of Technology, with a focus on the impact of intelligent transport systems on mobility. His research interest focuses on advanced driver assistance systems.

Barys Shyrokau received the Dipl.Eng. degree *(cum laude)* in mechanical engineering from Belarusian National Technical University, in 2004, and the joint Ph.D. degree in control engineering from Nanyang Technological University and Technical University Munich, in 2015. He is currently an Assistant Professor at the Section of Intelligent Vehicles, Department of Cognitive Robotics, Delft University of Technology. He is involved in the research related to vehicle dynamics and control, motion comfort, and driving simulator technology. He received the scholarship and award from FISITA, DAAD, SINGA, ISTVS, and CADLM.

Riender Happee received the M.Sc. degree in mechanical engineering and the Ph.D. degree from the Delft University of Technology (TU Delft), The Netherlands, in 1986 and 1992, respectively. He investigated road safety and introduced biomechanical human models for impact and comfort at TNO Automotive from 1992 to 2007. He is currently an Associate Professor at the Faculties of Mechanical, Maritime and Materials Engineering, and Civil Engineering and Geosciences, Delft University of Technology, where he investigates the human–interaction with automated vehicles focusing on safety, comfort, and acceptance.